



# High-rate biological selenate reduction in a sequencing batch reactor for recovery of hexagonal selenium

B. Song, Z. Tian, R.D. van der Weijden, C.J.N. Buisman, J. Weijma\*

Department of Environmental Technology, Wageningen University and Research, P.O. Box 17; 6700 AA Wageningen, the Netherlands

## ARTICLE INFO

### Article history:

Received 8 September 2020

Revised 30 December 2020

Accepted 16 January 2021

Available online 25 January 2021

### Keywords:

Biological selenate reduction

Ethanol

Selenium recovery

Selenite

Sequencing batch reactor

## ABSTRACT

Recovery of selenium (Se) from wastewater provides a solution for both securing Se supply and preventing Se pollution. Here, we developed a high-rate process for biological selenate reduction to elemental selenium. Distinctive from other studies, we aimed for a process with selenate as the main biological electron sink, with minimal formation of methane or sulfide. A sequencing batch reactor, fed with an influent containing 120 mgSe  $L^{-1}$  selenate and ethanol as electron donor and carbon source, was operated for 495 days. The high rates ( $419 \pm 17$  mgSe  $L^{-1} day^{-1}$ ) were recorded between day 446 and day 495 for a hydraulic retention time of 6 h. The maximum conversion efficiency of selenate amounted to 96% with a volumetric conversion rate of 444 mgSe  $L^{-1} day^{-1}$ , which is 6 times higher than the rates reported in the literature thus far. At the end of the experiment, a highly enriched selenate reducing biomass had developed, with a specific activity of  $856 \pm 26$  mgSe $^{-1} day^{-1} g_{biomass}^{-1}$ , which was nearly 1000-fold higher than that of the inoculum. No evidence was found for the formation of methane, sulfide, or volatile reduced selenium compounds like dimethyl-selenide or  $H_2Se$ , revealing a high selectivity. Ethanol was incompletely oxidized to acetate. The produced elemental selenium partially accumulated in the reactor as pure ( $\geq 80\%$  Se of the total mixture of biomass sludge flocs and flaky aggregates, and  $\sim 100\%$  of the specific flaky aggregates) selenium black hexagonal needles, with cluster sizes between 20 and 200  $\mu m$ . The new process may serve as the basis for a high-rate technology to remove and recover pure selenium from wastewater or process streams with high selectivity.

© 2021 The Author(s). Published by Elsevier Ltd.

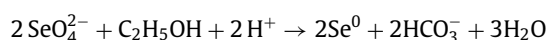
This is an open access article under the CC BY license (<http://creativecommons.org/licenses/by/4.0/>)

## 1. Introduction

Anthropogenic activities have dramatically increased selenium emissions, especially in the mining and metallurgical industries (Etteieb et al., 2020). Although selenium (Se) is an essential micronutrient for animals and humans, it is toxic at slightly higher intake levels than metabolically needed (Rayman, 2012; Ullah et al., 2018). Selenate ( $SeO_4^{2-}$ ), the prevailing Se species in discharged industrial effluents (He et al., 2018), accumulates in aquatic ecosystems, causing severe environmental impacts such as reproductive and teratogenic defects of aquatic life (Lemly, 2004).

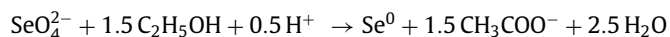
A promising method to eliminate selenate from industrial effluents is the microbiological reduction to elemental selenium ( $Se^0$ ) under anaerobic conditions. Technologies based on this concept can successfully remove selenate down to low ppb levels (Lenz et al., 2008a; Staicu and Barton, 2017; Tan, 2018).

With ethanol as an electron donor, the selenate reduction reaction is:



$$\Delta G_r^0 = -828 \text{ KJ mol}^{-1} \quad (1)$$

Or, when ethanol is partially oxidized to acetate:



$$\Delta G_r^0 = -444 \text{ KJ mol}^{-1} \quad (2)$$

However, for these biological methods still some issues remain, in particular the relatively low volumetric selenate conversion rate in bioreactors, with a reported maximum of only 72 mgSe  $L^{-1} day^{-1}$  (Ontiveros-Valencia et al., 2016). (Hageman et al., 2013) reported a rate of 104 mgSe  $L^{-1} day^{-1}$ , but most selenate (95%) was only partially reduced to selenite ( $SeO_3^{2-}$ ) and was therefore not removed from the solution. Although selenate displays a similar chemical behavior as sulfate, volumetric selenate reduction rates in bioreactors are up to 100 times lower than for biological sulfate

\* Corresponding author.

E-mail address: [jan.weijma@wur.nl](mailto:jan.weijma@wur.nl) (J. Weijma).

reduction (Liamleam and Annachhatre, 2007). Especially at higher selenate concentrations, such as in effluents from the selenium and copper refining industry (Ike et al., 2017), it becomes relevant to reach higher bio-reduction rates.

Another issue is the poor recovery of the final selenium products. Selenate bio-reduction at ~pH 7.0 and temperatures of up to 30 °C was reported to result in the formation of red amorphous  $\text{Se}^0$  particles with an estimated average size of 250 nm (Astratinei et al., 2006; Hageman et al., 2017a; Staicu et al., 2015), while intermediates form spheres to acicular selenium particles at pH 7.4–8 at 30 °C (Hageman et al., 2017a).  $\text{H}_2\text{Se}$  and organic Se compounds may form under highly reducing conditions (Lenz et al., 2008b; Nancharaiah and Lens, 2015). The selenium content of the generated suspended solids is often low, as it may also contain methanogenic and sulfate-reducing biomass, inorganic precipitates that have formed in the anaerobic reactor, or organic matter (Table 2). This hinders the recycling of the selenium product, which is relevant as selenium represents a potentially scarce element in the future (Weijden et al., 2013). Moreover, storing selenium-containing solid residues results in environmental risks when the selenium is remobilized under oxic conditions (Staicu et al., 2015; Zhang et al., 2004).

Here, we aimed to obtain a high-rate and highly selective process for biological selenate reduction from simulated selenate waste streams in order to generate a selenium solid product with relatively high purity. For this purpose, a sequencing batch reactor (SBR), which has been studied for selenate removal with ammonium removal (Mal et al., 2017) or nitrate removal (Kim et al., 2020) and has been reported to be able to rapidly enrich selenate-reducers (Kim et al., 2020), was operated at pH 7.5, fed with an influent containing up to 120 mgSe  $L^{-1}$  as selenate. Furthermore, we aimed to produce settleable selenium crystals or clusters thereof, which are relatively easy to separate from the aqueous phase.

## 2. Materials and methods

### 2.1. Source of biomass

The microbial inoculum consisted of anaerobic granular sludge, originating from a full-scale UASB reactor treating wastewater from a paper factory in Eerbeek, the Netherlands (Hageman et al., 2017a; Hulshoff Pol et al., 2001). Sludge from this reactor is mainly methanogenic but also has sulfate-reducing activity. The microbial composition of sludge from this reactor has been investigated previously (Roest et al., 2005; Tan et al., 2018b). The biomass was stored at 4°C before inoculation of the reactor and was therefore not adapted to selenate.

### 2.2. Medium composition

The basal medium used as influent for the bioreactor was adapted from Stams et al. (1992), omitting sodium selenite, sodium sulfide, and yeast extract (Stams et al., 1992). The medium consisted of (g  $L^{-1}$ ):  $\text{NaHCO}_3$  (4),  $\text{Na}_2\text{HPO}_4 \cdot 2\text{H}_2\text{O}$  (0.53),  $\text{KH}_2\text{PO}_4$  (0.41),  $\text{NH}_4\text{Cl}$  (0.3),  $\text{CaCl}_2 \cdot 2\text{H}_2\text{O}$  (0.11),  $\text{MgCl}_2 \cdot 6\text{H}_2\text{O}$  (0.10), and acid- and base trace elements and vitamin solution (Stams et al., 1992). Sulfate was not added to the influent medium until day 66 in order to suppress the growth of sulfate-reducing bacteria, which are known to be present in the inoculum sludge (Hageman et al., 2013). From day 66 onwards, around 142 mg  $L^{-1}$   $\text{Na}_2\text{SO}_4$  was added to the medium to provide sulfur as a nutrient for biomass growth. Ethanol was added as the electron donor to the medium. The reagents were of analytical grade unless stated otherwise.

### 2.3. Reactor setup

A reactor with a working volume of 0.40 L was operated in sequencing batch mode with four stages: feeding, mixing, settling, and discharging (Figure S1, SI).

The reactor temperature was controlled at 30 °C using a water bath. Nitrogen gas was bubbled continuously through the reactor solution at a rate of 0.02 mL  $s^{-1}$  to maintain anoxic conditions. The pH of the reactor solution was measured with a 210 mm glass S8 pH electrode (QP181X/210) and kept at  $7.5 \pm 0.1$  by a pH controller. The redox of the reactor liquid was measured from day 220–495 of the experiment with a 210 mm glass S8 Pt-billet redox electrode against Ag/AgCl and monitored with a PHM 210 Radiometer. The hydraulic retention time of the SBR was 24 h during day 0–351, 12 h during day 352–413, 6 h during day 414–419, 12 h during day 420–427, and 6 h until the end of the experiment.

The following operational disturbances occurred that temporarily affected the reactor performance in terms of selenate reduction: day 146–160: influent tubing clogged, day 186–204: air leakage, day 259–266: too much (8 mL) of 70% ethanol (v/v) as influent to the reactor on day 259 and reactor leakage on day 263, day 311–331 & day 358–363: feed pump failure and influent clogging, day 433 & day 463 & day 478–482: influent clogging.

Two gas scrubbers were connected to the gas outlet of the reactor. The first scrubber contained 200 mL of concentrated ethylene glycol (AllRide coolant, Newco Europe UK Ltd, the Netherlands) to capture any volatile organic Se compounds, while the second scrubber contained 200 mL of 3 M KOH to capture any possibly formed  $\text{H}_2\text{Se}$  (Hageman et al., 2013).

### 2.4. Batch experiments

Utilization of the electron donors ethanol and  $\text{H}_2$  by reactor sludge in the presence of selenate was assessed on day 498. For each experiment, a volume of 20 mL well-mixed content (containing  $1163 \pm 21$  mgCOD  $L^{-1}$  acetate) from the reactor was incubated in 125 mL bottles with 60 mL of fresh medium containing selenate and sulfate to reach a starting concentration of 1.1 mmol  $L^{-1}$  selenate and 1 mmol  $L^{-1}$  sulfate (further composition of medium same as described in Section 2.2). In total 200 mL content was taken from the reactor for batch experiments.

The culture bottles were closed with a butyl rubber stopper, and aluminum crimp seal. The headspace was degassed to 0.5 atm and then gassed to 1.5 atm with 100%  $\text{N}_2$ , except the experiment with  $\text{H}_2$  as the electron donor, which was flushed with 80%  $\text{H}_2$  and 20%  $\text{CO}_2$ . This was repeated 5 times with a final overpressure of 0.2 atm. The bottles were incubated in a shaker (120 rpm) at 30 °C. The selenate, selenite, ethanol concentration in solution, and the headspace gas composition were regularly analyzed. Batch experiments were carried out in duplicate.

For comparing the COD change among experiments with different electron donors, the  $\text{H}_2$  concentration is also expressed as mgCOD  $L^{-1}$  (calculated based on the ideal gas law and related to the liquid volume).

We designed an additional experiment to further elucidate the reaction pathway. In this experiment, hydrogen was added in excess to an incubation also containing selenate, selenite, and furthermore biomass and medium. With an excess of hydrogen, the fermentation of ethanol to hydrogen and acetate becomes thermodynamically unfeasible (Conrad et al., 1986). Ethanol consumption in the presence of hydrogen supports the direct pathway, while the absence of ethanol consumption would support the indirect route.

After day 498, the reactor's biomass was transferred to a sealed culture bottle with 1.2 atm 100%  $\text{N}_2$  in the headspace. The culture bottle was stored at 4 °C, and 50% of the medium inside the bottle was refreshed every month. The medium contained 1.5 mmol  $L^{-1}$

sodium selenate, 1 mmol  $L^{-1}$  sodium sulfate, and 200 mgCOD  $L^{-1}$  ethanol. The other components of the medium were the same as described in Section 2.2.

The ethanol utilization route was assessed using biomass from the reactor stored at 4 °C for ~3 months. 1 mL well-mixed content (containing < 10 mgCOD  $L^{-1}$  ethanol and acetate) was incubated in 125 mL bottles with 30 mL of fresh medium containing ethanol, selenate, and sulfate, leading with a starting concentration of 191 mgCOD  $L^{-1}$  ethanol, 1.2 mmol  $L^{-1}$  selenate, and 1 mmol  $L^{-1}$  sulfate. The culture bottles were sealed as described above and filled with 1.5 atm 100%  $N_2$  in the headspace. The bottles were incubated in a shaker (120 rpm) at 30 °C. Liquid samples were taken on days 1, 3, and 5.

Afterward, 10 mL fresh medium was added to the culture bottles to mix with the residual components, and the headspace was refilled with 1.2 atm of 80%  $H_2$  and 20%  $CO_2$ . Therefore, the starting concentration in assays was 25 mgCOD  $L^{-1}$  ethanol, 84 mgCOD  $L^{-1}$  acetate, 1572 mgCOD  $L^{-1}$   $H_2$ , 0.74 mmol  $L^{-1}$  selenite, 0.34 mmol  $L^{-1}$  selenate, and 1 mmol  $L^{-1}$  sulfate. The bottles were incubated in a shaker (120 rpm) at 30 °C. Liquid samples and gas composition were analyzed on day 1 and 2.

To investigate the morphology change of the produced elemental selenium (phase V), we transported the upper liquid from the reactor to culture bottles and tracked the size and structure change of samples by microscope. 0.02%  $NaN_3$  was added to control experiments by mixing  $Se^0$ -laden effluent and  $NaN_3$  solution to inhibit microbial activity, and the  $NaN_3$  was refreshed every 3 days. The culture bottles were sealed as described above and kept anaerobic by filling the headspace with 100%  $N_2$ . The batch bottles were incubated in a shaker (120 rpm) at 30 °C. Samples of the mixed content were collected on day 3.

## 2.5. Analysis and calculation

Liquid samples were filtered (0.45  $\mu m$ ) before analysis. Ethanol and acetate concentrations were measured by gas chromatography (as described by (Hageman et al., 2017b)).  $CH_4$ ,  $CO_2$ , and  $N_2$  were analyzed by a gas chromatograph (Shimadzu GC-2010) containing Porabond Q and Molsieve 5A columns, and  $H_2$  was analyzed using gas chromatography (Hewlett-Packard 5890A) (as described by (van Eerten-Jansen et al., 2015)). The sulfide concentration was measured using a Hach Lange test LCK-635 and a Hach Lange Xion 500 spectrophotometer. When the sulfide concentration was lower than the detection limit of this method (0.1 mg  $L^{-1}$  sulfide), an additional analysis with lead(II) acetate paper (Merck, Darmstadt, Germany) was performed to check if trace sulfide levels (less than parts per billion) were present (de Rink et al., 2019; Ter Heijne et al., 2018).

The selenate, selenite, and sulfate concentrations were analyzed by ion chromatography (Dionex ICS 2100, Thermo Fisher Scientific, Waltham, MA, USA). The total selenium concentration was analyzed at wavelength 196 nm by inductively coupled plasma optical emission spectrometry (VISTA-MPX CCD Simultaneous, VARIAN co. equipped with an MPX megapixel detector). The samples for total selenium analysis were first digested with 10 mL aqua regia in a microwave (ETHOS EASY Advanced Microwave Digestion System, Milestone Srl, Italy). The solid samples were washed as described previously (Hageman et al., 2017a) and characterized by light microscopy with a Nikon Eclipse E400 (1000x magnification, Nikon, Tokyo, Japan), X-ray diffraction (XRD) on a Bruker D8 advanced diffractometer equipped with a Vantec position sensitive detector and with a  $Co K\alpha$  radiation ( $\lambda = 0.179$  nm) over a range of 10–90° in 0.02 step sizes with an integration time of 0.5 s, and scanning electron microscope (SEM, Magellan 400, FEI, Eindhoven, the Netherlands). For SEM analysis, samples were washed with Milli-Q water and dried at room temperature. The method for SEM

analysis was described previously (Mol et al., 2020). The chemical composition was analyzed by Energy-dispersive X-ray spectroscopy (EDX) using the Aztec X-Ray analyzer (Oxford Instruments Analytical, High Wycombe, England) with a resolution of 0.4 nA at 10 kV.

The biomass was collected from the reactor on day 220 and concentrated by centrifugation to remove the supernatant. The sample pellet was subsequently frozen by liquid nitrogen and stored at –80°C. The composition of the microbial community was analyzed by 16S rRNA Gene Amplicon Sequencing, as described previously (De Leeuw et al., 2020). The sequencing data were submitted to the ENA database, and the accession number for the presented 16S rRNA sequencing set is PRJEB41212.

The biomass concentration was measured as the total organic nitrogen using Dr. Lange cuvette test LCK138 (Hach Lange, Germany). The specific method was described previously (de Rink et al., 2019). The biomass formula is regarded as  $CH_{1.8}O_{0.5}N_{0.2}$ , thus the measured total organic nitrogen accounts for 11%<sub>w/w</sub> of the total weight biomass.

The difference between selenate load and the load of dissolved selenium (sum of selenate and selenite) in the effluent was regarded as the production of elemental selenium ( $Se^0$ ). This assumption is based on the finding in the literature that  $Se^0$  is the dominant product of biological selenate reduction under similar conditions (Table 2) and our experimental findings that  $Se^0$  was found to precipitate in the reactor as a final product and so that no volatile Se species were detected in the gas scrubbing solution of the reactor.

## 3. Results and discussion

### 3.1. Selenate conversion rate at HRT of 24 h

The reactor was inoculated with 5 g wet anaerobic granular 'Eerbeek' sludge and operated at a hydraulic retention time (HRT) of 24 h for the first 350 days, divided into 3 Phases (I-III). The results of the reactor performance are shown in Fig. 1A-D.

During the start-up (Phase I, day 0–100), the volumetric selenate conversion rate gradually increased until a fairly stable level of 25–34 mgSe  $L^{-1}$  day $^{-1}$  was reached from day 69 to 100. Although the influent contained 4 to 6-fold excess of ethanol-COD relative to the stoichiometric needed COD for complete selenate reduction (Fig. 1B), the selenate conversion efficiency was only 67–79%, with 7–14 mgSe  $L^{-1}$  still present in the effluent (Figure S3, SI). The low efficiency may have been caused by substrate limitation because ethanol was consumed entirely (data not shown), and the effluent acetate concentration remained below 15 mgCOD  $L^{-1}$  from day 69–100. Presumably, a large fraction of the ethanol-COD was converted to methane by the methanogenic consortia present in the inoculum. This is supported by the poor COD recovery, which remained below 50% in Phase I (Fig. 1D).

At the start of Phase II (day 100–225), the selenate load was doubled to 80 mgSe  $L^{-1}$  day $^{-1}$  while the ethanol load was increased by only 20% to 170 mg COD  $L^{-1}$  day $^{-1}$  (Fig. 1A, B), in an attempt to steer the competition for reducing equivalents from ethanol towards selenate reduction. Although the selenate conversion rate increased immediately, a fraction of selenate was only partially reduced to selenite (Fig. 1A). After stepwise decreasing the ethanol load to ultimately 60 mgCOD  $L^{-1}$  day $^{-1}$  on day 169, selenite formation further increased, with about 1/3 of the depleted selenate appearing as selenite (Fig. 1A). The ethanol load was increased stepwise to 150 mgCOD  $L^{-1}$  day $^{-1}$  from day 205–225, after which the selenite formation rate decreased to below 5 mgSe  $L^{-1}$  day $^{-1}$  while the selenate reduction rate increased.

The start of Phase III (day 225–350) was marked by a 50% increase of the ethanol and selenate load. Selenite was formed transiently (Fig. 1A) until day 254, and again after periods of oper-

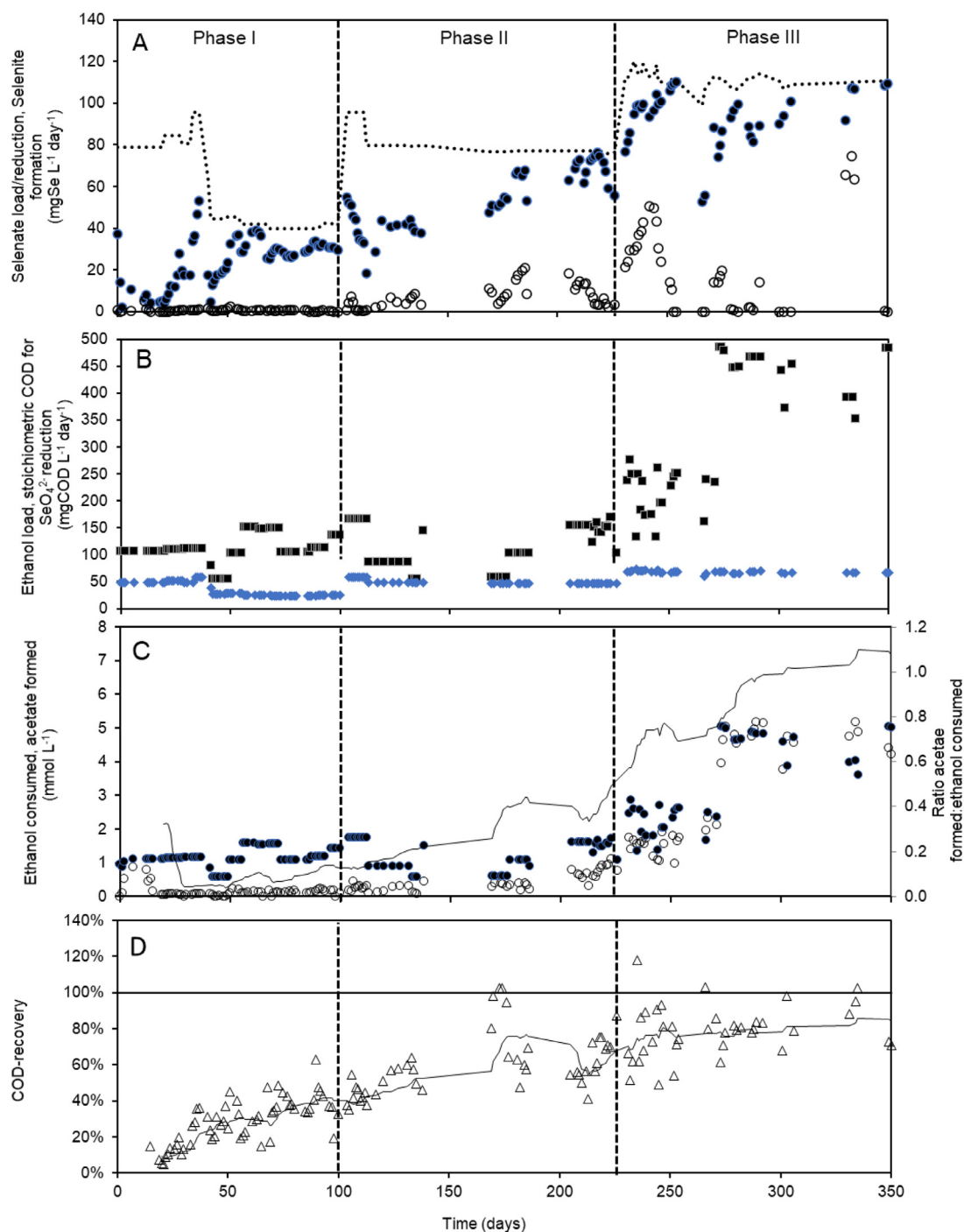


**Fig. 1.** Performance of the SBR for selenate conversion at HRT 24 h in Phase I-III. Legend: A)  $\circ$  - selenite formation rate,  $\bullet$  - selenate reduction rate,  $\bullet\bullet\bullet$  - selenate load; B)  $\blacksquare$  - ethanol load,  $\blacklozenge$  - stoichiometric COD load to selenate reduction; C)  $\circ$  - acetate formation,  $\bullet$  - ethanol consumption,  $--$  molar ratio acetate formed: ethanol consumed (moving average 10 datapoints); D)  $\triangle$  - COD recovery (moving average 10 datapoints); Note that operational disturbances (specified in methods section) on days 146–160, 186–204, 259–266, 311–331 temporarily affected reactor performance.

ational disturbances (day 259–266 and day 311–331). The reactor performance remained stable with a high conversion efficiency ( $\geq 94\%$ ) from day 332 to 350 with no selenite.

### 3.2. Selenate conversion rate at HRT of 12 and 6 h

Phase IV started with an HRT of 12 h and with a selenate and ethanol loading rate of 210–250  $\text{mgSe L}^{-1} \text{ day}^{-1}$  and 900–1100  $\text{mgCOD L}^{-1} \text{ day}^{-1}$ , respectively. The selenate conversion rate rapidly increased to levels close to the loading rate in two days,

with a conversion efficiency  $\geq 95\%$ . However, the selenate conversion rate started to decline after two weeks, while the selenite formation rate started to increase. This was thought to be caused by substrate limitation. Therefore the ethanol load was increased to 1920  $\text{mgCOD L}^{-1} \text{ day}^{-1}$  on day 387, resulting in a selenate conversion efficiency of  $\geq 95\%$  on day 413. Then it was tested whether this conversion efficiency would hold with low HRT at the start of Phase V (day 414), so the HRT was further decreased to 6 h. Within 1 day, the selenate conversion rate increased from 172 to 236  $\text{mgSe L}^{-1} \text{ day}^{-1}$  (conversion efficiency 65%), and further increased to 377

mgSe  $L^{-1}$  day $^{-1}$  (conversion efficiency 79%) on day 415. Yet, up to 25% of selenate was converted to selenite. Selenite formation kept increasing to 190 mgSe  $L^{-1}$  day $^{-1}$  even after doubling the ethanol load. To avoid the potential toxic effects of the high concentration of selenite on the microbial biomass (Hunter and Manter, 2009), the HRT was increased to 12 h for 1 week. The selenite formation rate dropped within 1 day to 8 mgSe  $L^{-1}$  day $^{-1}$  on day 422 and further decreased to below 0.5mgSe  $L^{-1}$  day $^{-1}$  on day 427. Meanwhile, the selenate conversion efficiency recovered to 98% on day 425 (rate 202 mgSe  $L^{-1}$  day $^{-1}$ ).

The HRT was again changed to 6 h on day 428. The selenate conversion rate first increased, while the selenite formation rate rapidly increased the following 5 days. Afterward, selenite formation decreased from 151 mgSe  $L^{-1}$  day $^{-1}$  (day 433) to only 1.5 mgSe  $L^{-1}$  day $^{-1}$  (day 450), while the selenate conversion rate gradually increased to around 440 mgSe  $L^{-1}$  day $^{-1}$  from day 446 to 495 (efficiency  $\geq$  90%). Several operational issues (see Materials and Methods section) resulted in the fluctuation of selenate reduction and selenite formation from day 450–490. The average selenate conversion rate was  $415 \pm 17$  mgSe  $L^{-1}$  day $^{-1}$  in this period, with effluent concentrations of 5–8 mgSe  $L^{-1}$  selenate and 0–3 mgSe  $L^{-1}$  selenite.

The average COD recovery in Phase IV and V was  $83 \pm 13\%$ , of which  $73 \pm 15\%$  was attributed to acetate formation and  $7.7 \pm 3.5\%$  to selenate reduction as either selenite or elemental selenium. In contrast with previous bioreactor studies, in our study, selenate reduction was independent of sulfate reduction. As sulfate reduction (the slight difference between sulfate inflow and outflow) and methanogenesis (no  $CH_4$  detected in headspace) were negligible, we presume that the 'missing' COD was covered by the unquantified microbial biomass production and possibly hydrogen formation (from ethanol fermentation). The latter could not be measured as it was purged from the solution and reactor with the nitrogen gas.

The maximum volumetric selenate conversion rate (444 mgSe  $L^{-1}$  day $^{-1}$ ) is around 6 times higher than previously reported (72 mgSe  $L^{-1}$  day $^{-1}$ , Table 2). When compared to previous research (Table 2), the relatively high selenate load in our study was achieved by using a low HRT in combination with a relatively high selenate concentration in the influent for a prolonged period. This enabled the development of a highly specific selenate reducing biofilm in the reactor. This would likely not have been possible with the low selenate concentration used in previous studies, as then unrealistically low HRTs would have to be applied. Interaction of sulfate and selenate reduction has been reported (Hockin and Gadd, 2006; Lenz et al., 2009; Tan et al., 2018a; Zehr and Oremland, 1987), but here the selenate conversion rate was not affected by sulfate reduction or the resulting potentially toxic sulfide (Lenz et al., 2008a) and therefore, there is no competition for electron donor. The low (or no) production of methane (also in the batch experiments) confirmed that mainly selenate is used in the reactor as the terminal electron acceptor by the specialized selenate reducing biomass.

### 3.3. Incomplete ethanol oxidation

During day 0–14 in Phase I, up to 55 mgCOD  $L^{-1}$  acetate was formed, but afterward, acetate formation remained low during Phase I (Fig. 1C), with concentrations below 15 mgCOD  $L^{-1}$ . In Phase II, the acetate concentration in the effluent gradually increased, while the molar ratio [acetate formed]:[ethanol consumed] increased to 0.5 (Fig. 1C), revealing partially incomplete oxidation of ethanol. This ratio further increased until it stabilized from day 275–350 with an average value of  $1.01 \pm 0.15$  [mol acetate produced]: [mol ethanol consumed], which revealed that all ethanol was incompletely oxidized to acetate. In period IV and V,

the molar ratio was  $1.14 \pm 0.23$ , also indicating incomplete ethanol oxidation. Thus, at the high rates observed in Phase III–V, selenate reduction proceeded according to Eq. (2). This is in line with thermodynamics, where the incomplete oxidation results in more Gibb's free energy change per electron ( $-74.0$  KJ mol $^{-1}$   $e^-$ ) than the complete oxidation of ethanol ( $-69.0$  KJ mol $^{-1}$   $e^-$ ) under actual reactor conditions.

### 3.4. Specific selenate reduction rate

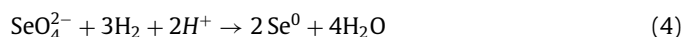
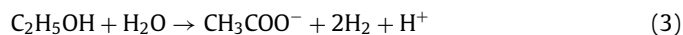
We attempted to monitor the biomass concentration based on the nitrogen content of suspended solids in the reactor. Unfortunately, a representative sampling from the reactor without opening the reactor proved impossible. To prevent exposing the biomass to oxygen (in the air), we refrained from opening the reactor. The biomass concentration at the start (day 0) and end (day 498) of the experiment amounted to 1.59  $g_{\text{biomass}} L^{-1}$  and 0.50  $g_{\text{biomass}} L^{-1}$ , respectively, corresponding to a 73% decrease. The specific selenate reducing activity of the inoculum, as assessed in a batch assay was  $0.82 \pm 0.06$  mg Se $^{-1}$  day $^{-1}$   $g_{\text{biomass}}^{-1}$ , while in the reactor at the end of the experiment it was  $856 \pm 26$  mg Se $^{-1}$  day $^{-1}$   $g_{\text{biomass}}^{-1}$ . The latter was based on the volumetric selenate reduction rate in the reactor during day 476 – 495 and the biomass concentration as assessed after the termination of the reactor experiment on day 495. Thus, the specific selenate reducing activity increased approximately 1000-fold during the almost 500-day experiment, indicating that selenate reducers were strongly enriched in the sludge.

The inoculum sludge originated from a full-scale anaerobic reactor treating paper factory wastewater and was predominantly methanogenic. The biomass collected at the end of the experiment did not produce measurable amounts of methane or sulfide in batch assays containing 0.12  $g_{\text{biomass}} L^{-1}$  within 72 h. Also, in the reactor, sulfate reduction was negligible (Figure S5, SI), while the high COD recovery of  $93 \pm 14\%$  (Fig. 2D) indicated that also methane formation did not contribute substantially as a sink for the electron donor.

In conclusion, the long-term experiment resulted in highly specific biomass, which incompletely oxidized ethanol, using selenate as the sole terminal electron acceptor.

### 3.5. Reaction route

In the reactor, ethanol may be directly used for selenate reduction (Eq. (2)), or ethanol may first be fermented to acetate and hydrogen (Eq. (3)), followed by the use of hydrogen by selenate reducing microorganisms (Eq. (4)).



To gain more insight into the ethanol degradation pathway, batch experiments with samples from the reactor taken on day 498 were carried out with either ethanol or hydrogen as added electron donor and selenate as the electron acceptor.

With  $740 \pm 5$  mgCOD  $L^{-1}$  ethanol, the molar ratio [acetate formed]:[ethanol consumed] was  $1.0 \pm 0.2$  after 24 h (Fig. 3B), confirming the incomplete oxidation of ethanol as already observed in the SBR, while hydrogen accumulated to  $0.55 \pm 0.02\%$  (v/v) in the headspace. These results indicated that ethanol is oxidized to acetate with  $H^+$  as an electron sink. Hydrogen decreased to  $0.036 \pm 0.003\%$  after 48 h, while the average molar ratio [acetate formed]:[ethanol consumed] increased to 1.34 ( $\pm 0.01$ ). Hydrogen composition further decreased to  $0.0008 \pm 0.01\%$  after 72 h while the molar ratio [acetate formed]:[ethanol consumed] was  $1.36 \pm 0.02$ , similar as after 48 h.

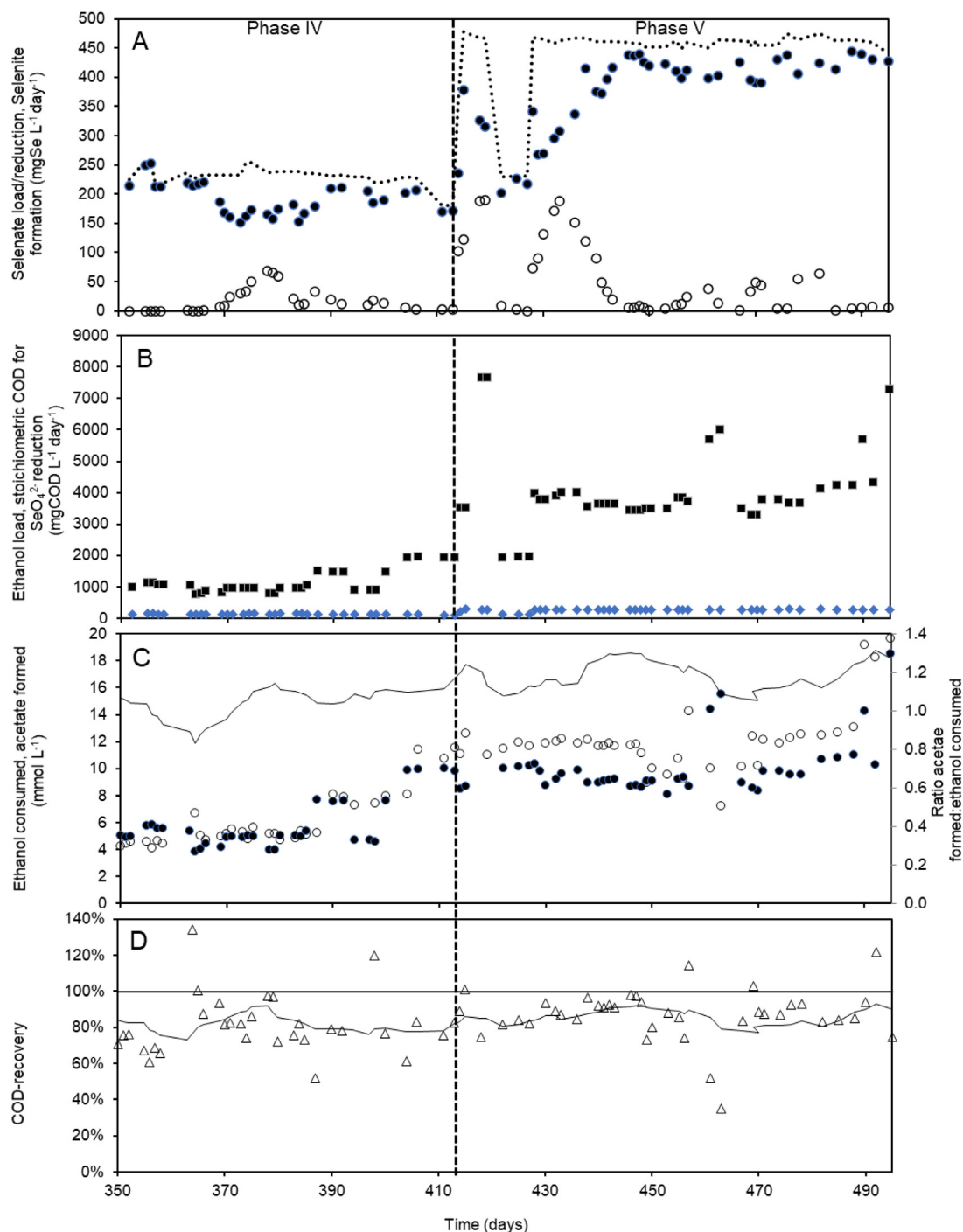


**Fig. 2.** Performance of the reactor for selenate conversion at HRT 12 h and 6 h. Legend: A) ○ - selenite formation rate, ● - selenate reduction rate, ●●●● - selenate load; B) ■ - ethanol load, ◆ - stoichiometric COD load to selenate reduction; C) ○ - acetate formation, ● - ethanol consumption, — - molar ratio acetate formed: ethanol consumed (moving average 10 datapoints); D) △ - COD recovery (moving average 10 datapoints). Note that operational disturbances (specified in methods section) on days 358–363, 433, 463, 478–482 temporarily affected the reactor performance.

Though the  $H_2$  concentration (Fig. 3B) decreased from 24 h to 72 h, the maximum measured  $H_2$  concentration was  $2.35 \pm 0.09$  mgCOD  $L^{-1}$  (at 24 h), which was less compared to the COD needed for selenate reduction. Thus, although this strongly supports that ethanol oxidation coupled to selenate reduction proceeded at least partially via hydrogen, we cannot exclude that ethanol was used also directly.

Unlike in the reactor, the larger part of the reduced selenate was converted to selenite (Fig. 3A). After a lag phase, the selenate depletion and selenite formation showed a linear trend from

16 to 48 h with a selenate depletion rate of  $43.2$  mgSe  $L^{-1}$  day $^{-1}$  ( $R^2=0.9963$ ) and a selenite formation rate of  $31.2$  mgSe  $L^{-1}$  day $^{-1}$  ( $R^2=0.9927$ ) respectively (Table 1). Thus, 73% of the depleted selenate was converted to selenite, while in the reactor, it was only 15% on the day of sampling of the microbial biomass (day 498). After 48 h, both the selenate conversion and selenite formation became slower, corresponding with the limitation of ethanol.

With  $H_2$  as electron donor ( $323$  mgCOD  $L^{-1}$  at the start), selenate was depleted within 72 h (Fig. 4) while the  $H_2$  concentration dropped to  $275 \pm 3$  mgCOD  $L^{-1}$ , providing further support for

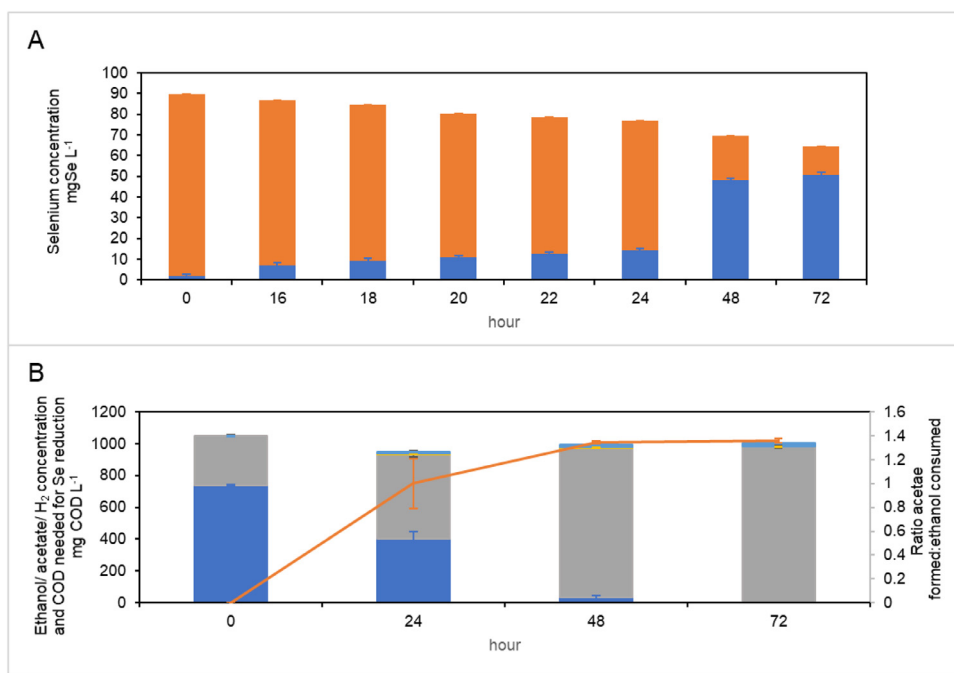


**Fig. 3.** Batch experiments with ethanol with well-mixed content from reactor. Legend: A) ■- selenite concentration, ■- selenate concentration; B) ■- acetate concentration, ■- ethanol concentration, ■- H<sub>2</sub> concentration, ■- COD needed for selenium reduction; — - molar ratio of formed acetate vs consumed ethanol. Conditions: 30 °C, pH 7.5, initial selenate concentration = 90 mg Se L<sup>-1</sup>, initial ethanol concentration = 740 ± 5 mgCOD L<sup>-1</sup>.

**Table 1**

Rates of selenate conversion and selenite and elemental selenium formation in experiments with different electron donors. Conditions: 30 °C, pH 7.5, initial selenite concentration: 90 mg Se L<sup>-1</sup>, using ethanol (740 ± 5 mgCOD L<sup>-1</sup>) or H<sub>2</sub> (323 mgCOD L<sup>-1</sup>) as electron donor.

mgSeL <sup>-1</sup> day <sup>-1</sup>	Average selenate reduction rate	Average selenite formation rate	Average Se <sup>0</sup> formation rate
with ethanol	42.7 (16–48 h)	31.2 (16–48 h)	–
with H <sub>2</sub>	52.5/43.5 (24–48 h)	34.3/ 31.5 (24–48 h)	19.4/ 12.5 (0–72 h)

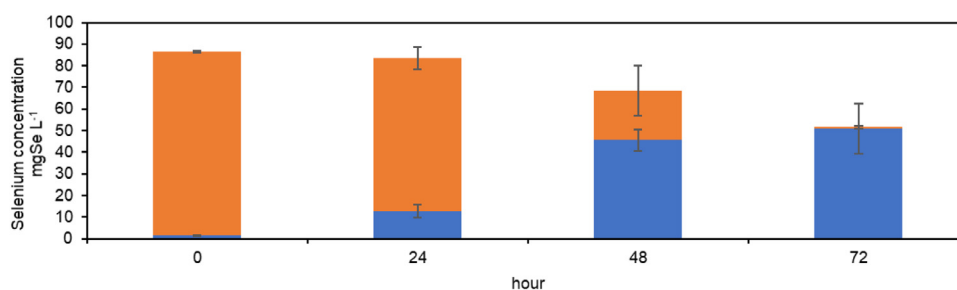


**Fig. 4.** Batch experiments using H<sub>2</sub> as electron donor with well-mixed content from reactor. Legend: ■- selenite concentration, ■- selenate concentration. Conditions: 30 °C, pH 7.5, initial selenate concentration = 90 mg Se L<sup>-1</sup>, initial H<sub>2</sub> concentration = 323 mgCOD L<sup>-1</sup>.

the hypothesis that hydrogen is an important contributing electron donor for selenate reduction in the reactor. It is noted that acetate was also present (314±1 mgCOD L<sup>-1</sup>) at the start, transferred together with the microbial biomass from the reactor. However, acetate did not serve as the electron donor for selenate reduction (315 ± 8 mgCOD L<sup>-1</sup> acetate after 72 h). On average 48 mgCOD L<sup>-1</sup> H<sub>2</sub> was consumed, of which 65% was covered by selenate reduction (to both selenite and elemental selenium).

Selenite was also found with hydrogen as the added electron donor. The calculated Se<sup>0</sup> production, which was based on the difference between selenate depletion and selenite formation, showed a linear trend from 24–72 h (Table 1 & Figure S6B1 and S6B2, SI), revealing that the Se<sup>0</sup> production was stable in the presence of both selenite and H<sub>2</sub>. The Se<sup>0</sup> production did not decrease when all selenate was depleted (<0.1 mmol L<sup>-1</sup>) after 72 h, indicating

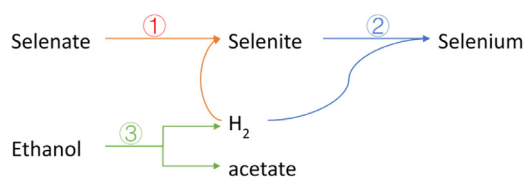


Fig. 5. Possible reaction route if the selenate reduction was achieved using the  $H_2$  produced by the ethanol fermentation.

that the  $Se^0$  may be formed solely by selenite reduction. Methane was not detected in any of the batches.

The results of the batch experiments using biomass from the reactor after storing at  $4^\circ C$  for  $\sim 3$  months are shown in Figure S8. With ethanol as the sole electron donor, the selenate was almost completely converted (to  $<0.03 \text{ mgSe L}^{-1}$  as selenate) in 5 days to selenite (84% of the total removed selenate) and elemental selenium while the ethanol was incompletely oxidized to acetate. Afterward, with ethanol and hydrogen, selenate was reduced with hydrogen being consumed while the ethanol concentration did not change. This result revealed that when hydrogen was present in excess, ethanol degradation is inhibited. This finding suggests that the indirect route, where hydrogen, formed from ethanol fermentation, serves as the electron donor for selenate reduction, is predominant.

Though hardly any literature reported this indirect-ethanol consumption pathway, the utilization of  $H_2$  as an electron donor (Chung et al., 2006; Huber et al., 2000; Lai et al., 2014; Ontiveros-Valencia et al., 2018, 2016; Pearce et al., 2008; Van Ginkel et al., 2011) or incomplete electron donor (lactate) oxidation (Fujita et al., 1997; Nancharaiah and Lens, 2015; Switzer Blum et al., 1998) for selenate or selenite reduction has already been studied. Selenite production as a final or intermediate selenate reduction product was also found (Astratinei et al., 2006; Chasteen and Bentley, 2003; Hageman et al., 2013; Switzer Blum et al., 1998).

Therefore, we may conclude that selenate reduction with selenite as an intermediated product is achieved using the  $H_2$  formed through the ethanol fermentation (Fig. 5). The transient accumulation of hydrogen in the batch experiments with ethanol and the inhibition of ethanol consumption by the excess presence of hydrogen points to the occurrence of this pathway. Furthermore, the initial accumulation of selenite indicates that selenate is first reduced to selenite (step 1, Fig. 5) and then to elemental selenium (step 2, Fig. 5).

### 3.5. Selenite formation in the reactor

The redox was monitored from day 220–495 (Fig. 6). Increases of the redox potential and selenite formation rate in the reactor experiment followed either after a process upset (redox/selenite formation peak 2, 3, 4, 5, 6, 7, 10, 11, and 12) or increase of the

selenate load (peak 1, 8, and 9). A concomitant increase of selenite accumulation and redox potential was also found in previous work (Hageman et al., 2013). After process upsets, the selenate reducing biomass may have been partially inhibited or may have decayed, resulting in a high load of selenate per number of active cells, which is the same effect after a sudden increase of the selenate load. Therefore, we speculate that a high ratio of [selenate load]:[active cells] triggers the inhibition of the reduction of selenite to elemental selenium, resulting in selenite accumulation. This would imply that selective selenite production from selenate might be achieved by controlling the redox, e.g., by maintaining substrate limiting conditions.

The insights gained from the batch experiments may also help to better explain the formation of selenite in the reactor (Fig. 1A and 2A).

### 3.6. Se speciation

Total selenium in the effluent was measured and shown for selected days (Fig. 7, selenate reduction rate  $>390 \text{ mgSe L}^{-1} \text{ day}^{-1}$ ). The total dissolved Se measured by ICP did not show much difference with the sum of selenate and selenite in the effluent (data not shown), indicating that no substantial other dissolved selenium species (selenide, organic selenium, or colloidal  $Se^0$ ) were formed. This is different from what Lenz found, where the dissolved selenium concentration was about three times higher than detected selenate concentration in the effluent (no selenite production), which was thought to have resulted from the formation of colloiddally dispersed  $Se^0$  nanoparticles (Lenz et al., 2008a). Thus, the slight differences between the total dissolved Se and Se oxyanions also exclude the production of colloiddally dispersed  $Se^0$ .

The difference between the total Se and total dissolved Se (sum of selenate and selenite) fluctuated from  $-3$  to  $11 \text{ mgSe L}^{-1}$ , indicating that a small fraction of the solid selenium washed out from the reactor. Indeed, red-colored particles, most likely amorphous selenium, were present in the SBR effluent, which could be removed by either  $0.45 \mu\text{m}$  filter or centrifugation. XRD analysis did not show any crystalline  $Se^0$  signal for washed-out particles, suggesting that the red selenium solids indeed were amorphous.

The increase of total washed out amorphous Se at day 471 could be attributed to mixing of the reactor prior to the attempted sampling for biomass density analysis, which may release attached amorphous elemental selenium. The short HRT in this phase (6 h) may be not feasible for settling of all the solids because  $\geq 5 \text{ mgSe L}^{-1}$  elemental selenium was washed out several days after the attempt for biomass density sampling (day 471–478), which was not seen in the case of 24 h or 12 h HRT ( $\leq 3 \text{ mgSe L}^{-1}$  before and after sampling, data not shown).

The total Se concentration in the gas scrubbing solutions was always lower than the detection limit ( $1 \text{ mgSe L}^{-1}$ ), indicating no organic Se or  $H_2Se$  was produced in the reactor.  $H_2Se$  was reported

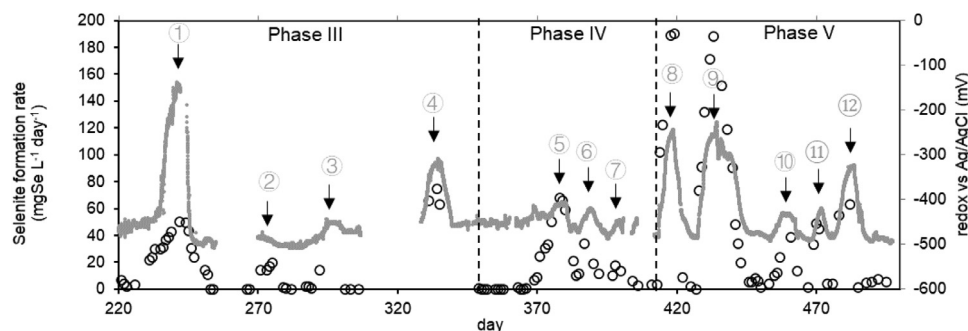
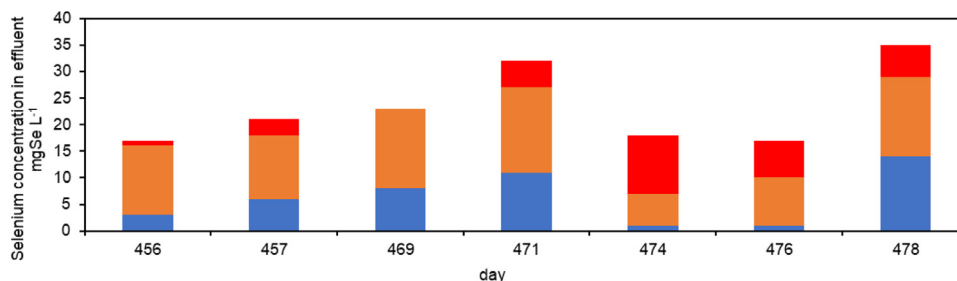


Fig. 6. The selenite formation rate and redox potential in SBR from day 220–495. legend: ....- redox potential, .....- selenite formation rate.



**Fig. 7.** Se speciation in SBR effluent on selected days (with selenate reduction rate  $>390 \text{ mgSe L}^{-1} \text{ day}^{-1}$ ) in Phase V. legend: ■ - selenite concentration, ■ - selenate concentration, ■ - calculated total solid phase selenium. The total solid phase selenium was calculated as the difference between the ICP results of total Se and total dissolved Se (sum of selenate and selenite). Conditions: selenate load =  $459 \pm 8 \text{ mgSe L}^{-1} \text{ day}^{-1}$ ; HRT = 6 h.

to be produced by SRBs (Nelson et al., 1996), and dimethylselenide and dimethyldiselenide were found to be produced by SRBs and methanogens (Michalke et al., 2000). The absence of volatile Se species in the SBR after the long-term operation points to the selection of specialized selenate and selenite reducers while the sulfate-reducing bacteria and methanogens from the original Eerbeek sludge were washed out.

The total dissolved selenium concentration was much higher than allowed according to the discharge limit ( $<50 \mu\text{g L}^{-1}$  as selenate, or  $<10 \mu\text{gSe L}^{-1}$  as total selenium) (Tan et al., 2016a). Still, the batch experiments showed the possibility to remove selenate to less than  $20 \mu\text{gSe L}^{-1}$  (detection limit) within 144 h and  $0.35 \mu\text{gSe L}^{-1}$  of selenite. The latter may be further reduced by extending of the reaction time.

### 3.7. Solids accumulation in the reactor

In Phase I, similarly to previous work, we found that the first formed Se solids using Eerbeek sludge were orange-red spherical amorphous selenium particles attached to the biomass (Hageman et al., 2017a). Because amorphous selenium is thermodynamically not the most stable phase, it was postulated that bacterial organic material (polysaccharides, polymers) attached to the selenium hinders crystallization to hexagonal selenium (Hageman et al., 2017a; Lenz et al., 2011). As listed in Table 2, The amorphous  $\text{Se}^0$  attachment to biomass was found in various processes (Hageman et al., 2017a; Lenz et al., 2011, 2008a; Mal et al., 2017).

However, several factors in this system might still allow the formation and recrystallization of amorphous selenium into black hexagonal selenium; the pH, the accumulation of amorphous selenium in the reactor increasing the probability of aggregation, and the driving force to obtain the thermodynamically most stable phase. First of all, the pH in our experiments was 7.5, and according to Hageman's findings, with increasing pH from pH 7 onwards, he found black hexagonal selenium forms already at a pH of  $\sim 7.4$  (Hageman et al., 2017a). It is reported that the surface potential of biopolymers would become more negative with pH increase (Carneiro-Da-Cunha et al., 2011); the same is true for proteins (Schmitt et al., 1998). Therefore, there is more likely that the selenium particles detach from the negatively-charged bacteria. Besides, the sorption affinity of proteins and lipopolysaccharides (LPS) to selenium surfaces may decrease with an increase in pH (Parikh and Chorover, 2008).

The accumulation of amorphous Se particles resulting from feeding the reactor with high selenate concentrations can then promote the aggregation. It is reported that the organics tend to detach from the inorganic materials, allowing the formation of a larger structure because Brownian motion-driven particle collisions, decreasing the effective surface area with the solution, would overcome the surface tension energy allowing crystalliza-

tion (Banfield et al., 2000). Hence, the (re)crystallization and transformation to the most stable phase is allowed (Banfield et al., 2000; Jin et al., 2018), which can lead to larger organized single crystals as mentioned in a comment on the work by Banfield et al. (2000) (Alivisatos, 2000).

The aggregation of selenium particles has already been reported previously (Hageman et al., 2017a). Besides, the observation of morphology changes of the solids from amorphous round to acicular crystalline phases was confirmed in batch experiments where biomass activity was inhibited with  $\text{NaN}_3$ , indicating an abiotic process after biomineralization of amorphous selenium. Figure S9A showed how sphere particles aggregated with the existed acicular clusters on day 3. The overview picture of the particles (Figure S9B) showed that generally quantity and size of the clusters increased when sampled from day 3 to day 30. One may note that this batch experiment was carried out in phase V when the reactor has already operated continuously for  $\sim 500$  days; it is reasonable to find several large acicular clusters at the beginning of batch assays. With the picture shown in Figure S9B, we speculated both size and numbers of acicular particles in the aggregates increased with time.

Furthermore, attachment to reactor walls and tubing enhances this aggregation and recrystallization process as the attachment also decreases the surface tension energy that has to be overcome, probably therefore, we found the black hexagonal selenium on the tubing and reactor walls. As systems tend to progress to the most stable thermodynamic state, then recrystallization leads to black hexagonal selenium; recrystallization is based on both the Ostwald step rule (going from amorphous to crystalline state) and Ostwald ripening (small particles merge/recrystallize to large particles as to reduce surface area (i.e., aging). The longer the SRT in the reactor, the more time for Ostwald processes, and the more likely black hexagonal selenium will make up the bulk of the solids found in the reactor.

It is also reported that the attachment of  $\text{Se}^0$  to the sludge leads to faster settling rates and higher hydrophilicity compared with sludge without entrapment  $\text{Se}^0$  (Jain et al., 2015), which helps capture the produced amorphous  $\text{Se}^0$  in the reactor. The sequence batch mode was also reported to benefit the settling of the produced  $\text{Se}^0$  (Mal et al., 2017). As a result, red color was observed in the sludge and on the reactor wall in the first stages of the experiment.

After day 100 (in Phase II), more of the reactor wall area was covered with solids, and the color changed from red to black. Dried macroscopic flakes from the  $\text{N}_2$  tubing on day 229 had a metallic luster. These consisted of clusters of needles with a size ranging between 20 and 200  $\mu\text{m}$ . The cluster (Fig. 8A) is remarkably similar to the cluster of the selenium particles found on day 195 in a thermophilic ( $50 \text{ }^\circ\text{C}$ ) selenate reducing reactor (Hageman et al., 2015), but the reduction rate in our case was much higher than in the thermophilic reactor ( $5\%$  of  $1 \text{ mmol L}^{-1}$  selenate). The length of

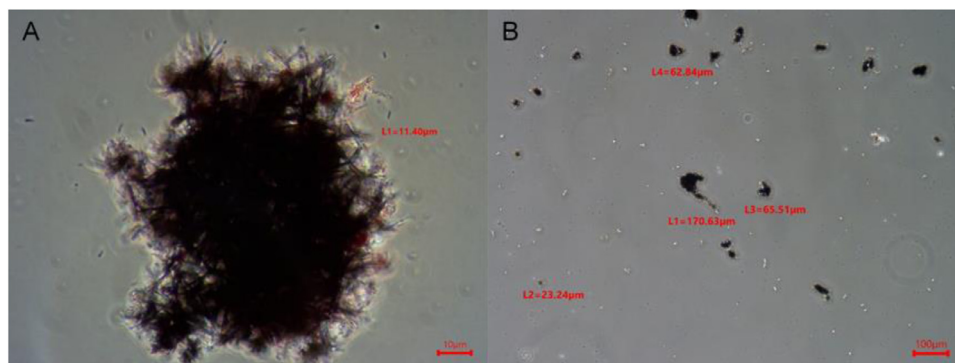


**Fig. 8.** Solids from the bottom of the reactor and N<sub>2</sub> tubing were analyzed by the light microscope from day 229 (only image on day 393 (A) and 453 (B) was shown). (A) a cluster of acicular-like particles with a length of each individual needle at about 10 μm; (B) mixture of needle clusters with a size ranging between 20 and 200 μm.

an individual needle was approximately 10 μm. This result is similar to the size that Hageman et al. found for pH 8 but somewhat smaller than at pH 9 (Hageman et al., 2017a).

After 495 days, flaky aggregates (>1 mm) of black solids attached to the N<sub>2</sub> tubing, solids that had settled at the bottom of the reactor, solids attached to the reactor wall, and suspended solids were collected. With ICP, the total Se content in the solid materials from the bottom of the reactor was 80% (0.8 g Se g<sup>-1</sup> dry solid). These solid materials were a mixture of biomass sludge flocs and flaky selenium aggregates. More specifically, the flaky aggregates (not only mixed with biomass in the bottom but also attached to N<sub>2</sub> tubing or the reactor wall) contained ~100% pure Se (~1 g Se g<sup>-1</sup> dry solid). These Se aggregates are more hydrophobic, more adamant, and constitute the largest mass fraction in the sludge. The larger particle sizes of these aggregates compared with biomass make them easily separable from biomass by mesh sieves (Ruiken et al., 2013). The density of pure hexagonal selenium is also high (4.81 g/cm<sup>3</sup>), so separation by gravitational methods (i.e., centrifugation (Hageman et al., 2017a), hydrocycloning (Coffey, 2009), microbubble flotation (Yoon, 1993) or sed-

imentation) may also be applicable. The formation of pure (≥80% of total mixed solids) large selenium precipitates has not yet been reported in the literature (Table 2). The solid mixture in the bottom contained 67 g Se (6.7 g Se mL<sup>-1</sup> of in total of ~10 mL solids), which is 87% w/w of the calculated total selenate load to the reactor during the experiment (77 g Se, calculated value). One may note that the start-up of this process (day 0–50) and during some operational disturbances, the reactor had relatively low selenate removal efficiency, which was also included in the calculation. Thus, we may conclude that the Se recovery potential of this process is ≥87%.

An increase in the retention of solids (amorphous and hexagonal) in the reactor could be achieved by an increase in the surface area for Se<sup>0</sup> attachment (for instance, by adding more supporting material inside the reactor) and an increase in the settling time compared to the stirring time, which were 2 and 34 min, respectively, repeated in cycles of 40 min.

For phase analysis of the black needles sampled from the reactor, XRD (on day 240) and SEM-EDX (on day 287) were used. The XRD spectra (Fig. 9) matched with the hexagonal crystalline Se

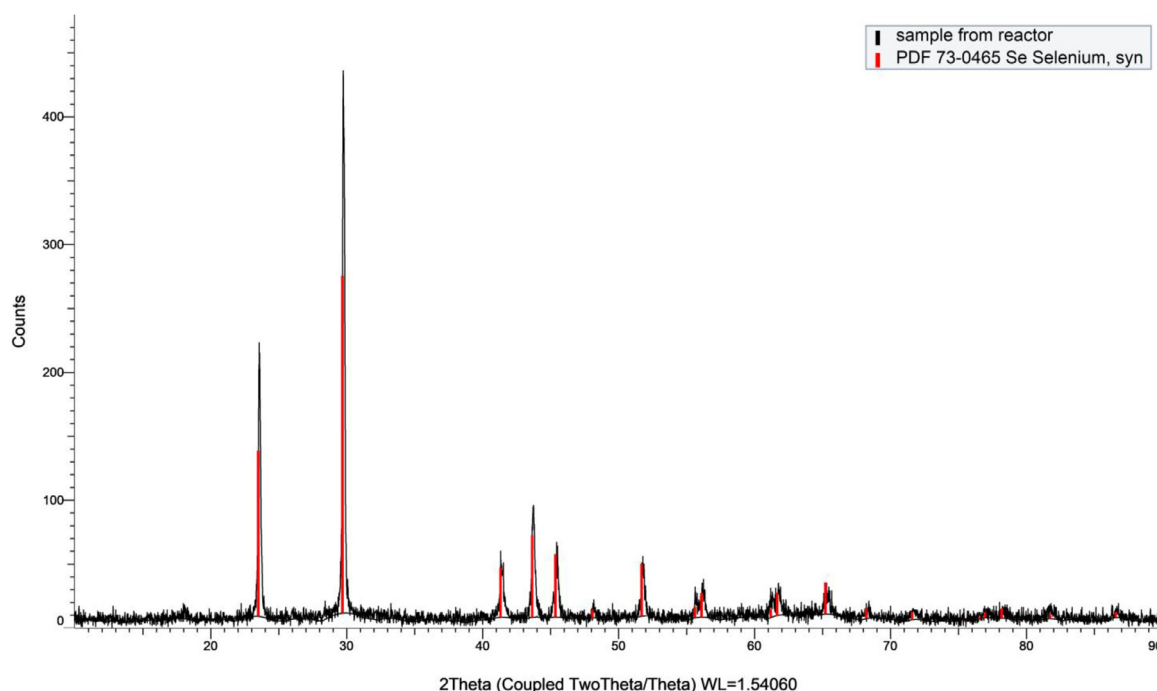


**Fig. 9.** XRD diffractograms of solids from Reactor (day 240) confirmed the presence of hexagonal elemental selenium.

**Table 2**  
A summary of selenate conversion in mesophilic (25–35 °C) bioreactors operated at circumneutral pH (7–8) reported in literature.

Reactor type	T °C	HRT h	pH	e-donor	SeO <sub>4</sub> <sup>2-</sup> influent mgSe L <sup>-1</sup>	SeO <sub>4</sub> <sup>2-</sup> conversion rate mgSe L <sup>-1</sup> day <sup>-1</sup>	SeO <sub>4</sub> <sup>2-</sup> conversion efficiency	SO <sub>4</sub> <sup>2-</sup> influent mg L <sup>-1</sup>	NO <sub>3</sub> <sup>-</sup> influent mg L <sup>-1</sup>	Se solid phase	reference
SBR	30	6	7.5	ethanol	120	up to 444	≤96%	96	0	black crystalline hexagonal Se <sup>0</sup>	This paper
SBR	30	48	not specified	acetate	0.79–79	39.5	~100%	99	62	not specified	(Kim et al., 2020)
SBR	30	12	7.0–7.1	acetate	1	1.94	≤97%	16	0	amorphous Se <sup>0</sup> in sludge	(Mal et al., 2017)
MBFR <sup>2</sup>	25	3.3	not specified	H <sub>2</sub>	1–11	72	90%	0–90	4.4	Se <sup>0</sup> aggregates	(Ontiveros-Valencia et al., 2016)
Drip flow reactor	30	5.8 <sup>1</sup>	7–8	acetate	10.27	32	76%	1238	298	spherical Se <sup>0</sup> nanoparticles	(Tan et al., 2018)
UASB <sup>3</sup>	30	6	7	lactate	0.79	3	97–99%	≤ 2496	0	amorphous Se <sup>0</sup> in sludge	(Lenz et al., 2008)
UASB	30	12	7–7.5	lactate	10	20	99.9%	0	0	red Se <sup>0</sup> and metal-selenide	(Zeng et al., 2019)
MBFR	24–26	5.2	7.5	H <sub>2</sub>	2	8.8	95%	nutrient level	44	amorphous Se <sup>0</sup>	(Xia et al., 2019)
Fed-batch	30	18	7	lactate	1975	60	98%	0	0	not specified	(Hageman et al., 2013)
UASB	30	12	7.3	lactate	3.95	6.5	82% (-NO <sub>3</sub> <sup>-</sup> )	0	up to 310	Se <sup>0</sup> nanoparticles	(Dessi et al., 2016)
IFBR <sup>4</sup>	35	120	6–7	ethanol	790	251	44% (+NO <sub>3</sub> <sup>-</sup> )	-	-	red Se <sup>0</sup>	(Cheng et al., 2017)

<sup>1</sup> EBCT = Empty Bed Contact Time.  
<sup>2</sup> MBFR = Membrane Biofilm Reactor.  
<sup>3</sup> UASB = Upflow Anaerobic Sludge Blanket.  
<sup>4</sup> IFBR = Inverse Fluidised Bed Reactor.

with a probability of 92%. With SEM (Fig. 10), the needle form can be distinguished, which is typical for hexagonal selenium, and EDX analysis confirmed that this acicular structure consisted of 100% Se. Therefore, after the initial precipitation of amorphous selenium in Phase I, crystallization to hexagonal elemental selenium has occurred. As the bioreactor is continuously precipitating new selenium, this could promote the growth of these needles.

### 3.8. Biomass community

We chose the Eerbeek inoculum based on its high microbial diversity (Roest et al., 2005) and applied selective conditions for over a year and a half, thereby aiming to select and enrich species that would be well-adapted.

Next generation sequencing (NGS) analysis of the biomass revealed that the community in the reactor (sampled at day 220, end of Phase II) was different from the biomass of the original Eerbeek sludge (Roest et al., 2005; Tan et al., 2018b). The biomass community was dominated by bacteria, and the most abundant microorganisms were from the *Proteobacteria* phylum (30% of the community sequences, Table S2 SI), followed by *Firmicutes* (17%) and *Bacteroidetes* (16%). Many reported selenate/selenite reducing bacteria distribute in the *Proteobacteria* (Knotek-Smith et al., 2006; Tan et al., 2016b). Though *Firmicutes* is known to contain sulfate-reducing species (Tan et al., 2018a), these are often also able to reduce selenate (Knotek-Smith et al., 2006; Tan et al., 2016b). *Bacteroidetes* are also believed to play a role in the reduction of selenium oxyanions as selenate reductase was identified in the genomes of this phylum (Fakra, 2015).

*Geobacteraceae* is the most abundant family, representing 16% of total community families identified. There are various members of this family known as metal reducers, and selenite is included (Nancharaiah and Lens, 2015; Pearce et al., 2009; Tan et al., 2018a). For instance, Strain KM<sup>T</sup> was reported to be able to use acetate to reduce selenate and selenite (Nasaringarao and Häggblom, 2007).

More specifically, *Geobacter* accounted for 16% of the total genera identified. One member of this genus, *Geobacter sulfurreducens* PCA, was reported to couple hydrogen or acetate oxidation with selenite respiration (Nancharaiah and Lens, 2015; Pearce et al., 2009).

The most abundant archaeal group was *Methanosaetaceae* (6% of the total microbial families), which are known acetotrophic methanogens. On the day of sampling (day 220), the molar ratio [acetate formed]:[ethanol consumed] was 0.5, suggesting that 50% of the acetate was still consumed by the reactor biomass. Likely, the acetate was converted to (undetected) methane as indicated by the low COD recovery of around 60% on day 220. The increase in the molar ratio [acetate formed]:[ethanol consumed] and the COD-recovery to approximately 1.0 and 80–90% respectively, from day 280 onwards, indicate that the acetotrophic methanogens gradually washed out or became inactive.

*Desulfuromonadaceae*, which are known as sulfate/sulfur reducers, was found to contribute to 5% of the population. However, hardly any sulfate concentration change was found in the effluent (Figure.S5, SI). Many sulfate reducers also reduce selenate, which may explain their presence.

As so, many members from the abundant phylum are found to be related to selenate/selenite reduction, we may conclude that during the 495 days of the microbial community development, microbes that are well-adapted to the selenium reduction were selected. This is in line with the satisfying reactor performance of on the average 97% selenate selectivity before the sampling date (day 216–219). The increased COD recovery in Phase I-III and the negligible methane production or sulfate reduction (as discussed before in Section 3.4) is also due to the biomass community change.

The strategy of a) starting with a rich community and b) applying selective conditions for a prolonged period has proven success-

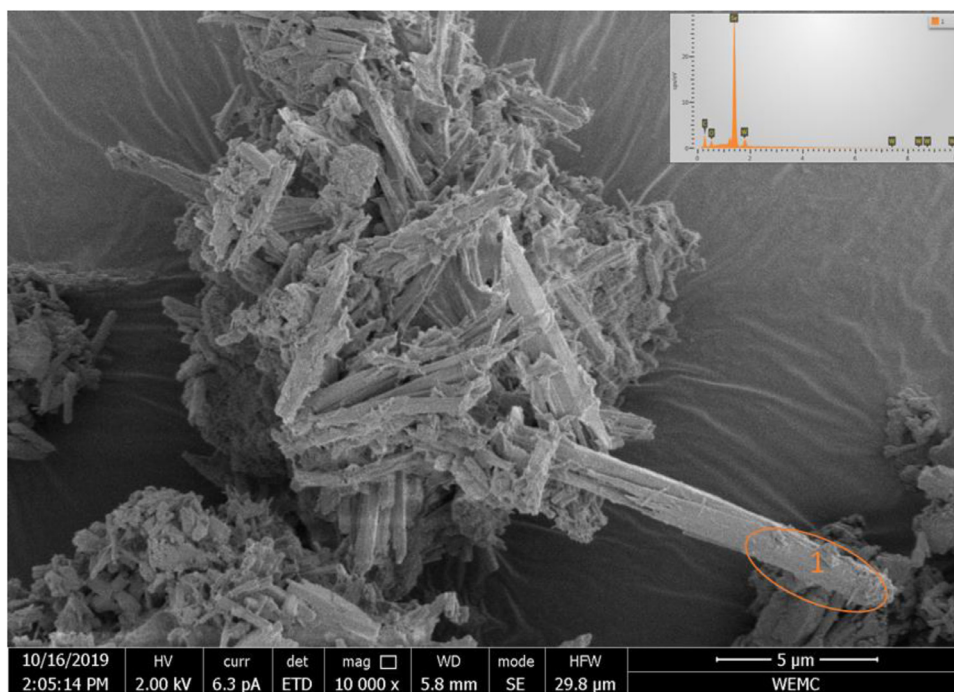


**Fig. 10.** Evaluation and characterization of the black needles sampled from the bottom of the reactor on day 287. Acicular-like solid was distinguished by SEM image (left) and the chemical composition of the selected area (labeled as 1) was analyzed by EDX (top-right) confirmed the needle consisted of 100% selenium.

ful in our environmental biotechnological research (Hageman et al., 2013; Lindeboom et al., 2011; Weijma et al., 2000). Still, by default, we cannot exclude that other inocula would have led to the same biomass development or even higher selenate reduction rates.

#### 4. Conclusion

This study presented a high-rate process for the recovery of selenium based on biological selenate reduction to elemental selenium without the formation of highly toxic hydrogen selenide or organic selenium species. Pure crystalline hexagonal  $\text{Se}^0$  was identified as selenium solid accumulating in the reactor in clusters and was easy to separate. The achieved high purity would facilitate the recycling of the generated selenium. Selenate was the predominant electron acceptor in the process, while  $\text{CO}_2$  and sulfate reduction were absent. However, ethanol was incompletely oxidized, implying that maximally 1/3 of the electron equivalents in ethanol could be used for the desired conversion. Selenite was found both in reactor and batch experiments, revealing the presence of selenite as intermediate being produced from selenate. This process can be used for high concentrated process and waste streams.

#### Declaration of Competing Interest

The authors declare that they have no known competing financial interests or personal relationships that could have appeared to influence the work reported in this paper.

#### Acknowledgements

**Funding:** This work was supported by the Netherlands Enterprise Agency's TKI program, within the project Biocrystallization of Selenium down to ultra-low levels, with number 2016WUR003 and the student was supported by the China Scholarship Council.

We thank Marcel Giesbers from the Wageningen Electron Microscopy centre for helping with the SEM pictures and Zoe Spencer for helping with the grammar.

#### Supplementary materials

Supplementary material associated with this article can be found, in the online version, at doi:10.1016/j.watres.2021.116855.

#### References

- Alivisatos, A.P., 2000. Naturally aligned nanocrystals. *Science* (80-) 289. doi:10.1126/science.289.5480.736, 736 LP – 737.
- Astratinei, V., Van Hullebusch, E., Lens, P., 2006. Bioconversion of selenate in methanogenic anaerobic granular sludge. *J. Environ. Qual.* 35, 1873. doi:10.2134/jeq2005.0443.
- Banfield, J.F., Welch, S.A., Zhang, H., Ebert, T.T., Penn, R.L., 2000. Aggregation-based crystal growth and microstructure development in natural iron oxyhydroxide biomineralization products. *Science* (80-) 289, 751–754. doi:10.1126/science.289.5480.751.
- Carneiro-Da-Cunha, M.G., Cerqueira, M.A., Souza, B.W.S., Teixeira, J.A., Vicente, A.A., 2011. Influence of concentration, ionic strength and pH on zeta potential and mean hydrodynamic diameter of edible polysaccharide solutions envisaged for multilayered films production. *Carbohydr. Polym.* 85, 522–528. doi:10.1016/j.carbpol.2011.03.001.
- Chasteen, T.G., Bentley, R., 2003. Biomethylation of selenium and tellurium: microorganisms and Plants. <https://doi.org/10.1021/cr010210>
- Chung, J., Nerenberg, R., Rittmann, B.E., Jinwook, C., Robert, N., Bruce, E., Rittmann, C.J., Nerenberg, R., Rittmann, B.E., 2006. Bioreduction of selenate using a hydrogen-based membrane biofilm reactor. *Environ. Sci. Technol.* 40, 1664–1671. doi:10.1021/es051251g.
- Coffey, M., 2009. Energy and power generation: maximising biogas yields from sludge. *Filtr. Sep.* 46, 12–15. doi:10.1016/S0015-1882(09)70085-0.
- Conrad, R., Schink, B., Phelps, T.J., 1986. Thermodynamics of  $\text{H}_2$ -consuming and  $\text{H}_2$ -producing metabolic reactions in diverse methanogenic environments under in situ conditions. *FEMS Microbiol. Lett.* 38, 353–360. doi:10.1111/j.1574-6968.1986.tb01748.x.
- De Leeuw, K.D., De Smit, S.M., Van Oossanen, S., Moerland, M.J., Buisman, C.J.N., Strik, D.P.B.T.B., 2020. Methanol-based chain elongation with acetate to n-butyrate and isobutyrate at varying selectivities dependent on pH. *ACS Sustain. Chem. Eng.* 8, 8184–8194. doi:10.1021/acssuschemeng.0c00907.
- de Rink, R., Klok, J.B.M., van Heeringen, G.J., Sorokin, D.Y., ter Heijne, A., Zeijlmaaker, R., Mos, Y.M., de Wilde, V., Keesman, K.J., Buisman, C.J.N., 2019. Increasing the selectivity for sulfur formation in diverse methanogenic environments. *Environ. Sci. Technol.* 53, 4519–4527. doi:10.1021/acs.est.8b06749.
- Etteieb, S., Magdoui, S., Zolfaghari, M., Brar, S., 2020. Monitoring and analysis of selenium as an emerging contaminant in mining industry: a critical review. *Sci. Total Environ.* 698, 134339. doi:10.1016/j.scitotenv.2019.134339.
- Fakra, S.C., 2015. Spectro-microscopic studies of microbial selenium and iron reduction in a metal contaminated aquifer.

- Fujita, M., Ike, M., Nishimoto, S., Takahashi, K., Kashiwa, M., 1997. Isolation and characterization of a novel selenate-reducing bacterium, *Bacillus* sp. SF-1. *J. Ferment. Bioeng.* 83, 517–522. doi:10.1016/S0922-338X(97)81130-0.
- Hageman, S.P.W., van der Weijden, R.D., Stams, A.J.M., Buisman, C.J.N., 2017a. Bioproduction of selenium nanoparticles with diverse physical properties for recovery from water. *Int. J. Miner. Process.* 169, 7–15. doi:10.1016/j.minpro.2017.09.018.
- Hageman, S.P.W., van der Weijden, R.D., Stams, A.J.M., van Cappellen, P., Buisman, C.J.N., 2017b. Microbial selenium sulfide reduction for selenium recovery from wastewater. *J. Hazard. Mater.* 329, 110–119. doi:10.1016/j.jhazmat.2016.12.061.
- Hageman, S.P.W., van der Weijden, R.D., Weijma, J., Buisman, C.J.N., 2013. Microbiological selenate to selenite conversion for selenium removal. *Water Res.* 47, 2118–2128. doi:10.1016/j.watres.2013.01.012.
- He, Y., Xiang, Y., Zhou, Y., Yang, Y., Zhang, J., Huang, H., Shang, C., Luo, L., Gao, J., Tang, L., 2018. Selenium contamination, consequences and remediation techniques in water and soils: a review. *Environ. Res.* doi:10.1016/j.envres.2018.02.037.
- Hockin, S., Gadd, G.M., 2006. Removal of selenate from sulfate-containing media by sulfate-reducing bacterial biofilms. *Environ. Microbiol.* 8, 816–826. doi:10.1111/j.1462-2920.2005.00967.x.
- Huber, R., Sacher, M., Vollmann, A., Huber, H., Rose, D., 2000. Respiration of arsenate and selenate by hyperthermophilic archaea. *Syst. Appl. Microbiol.* 23, 305–314. doi:10.1016/S0723-2020(00)80058-2.
- Hulshoff Pol, L.W., Lens, P.N.L., Weijma, J., Stams, A.J.M., 2001. New developments in reactor and process technology for sulfate reduction. *Water Sci. Technol.* 67–76. doi:10.2166/wst.2001.0467.
- Hunter, W.J., Manter, D.K., 2009. Reduction of selenite to elemental red selenium by *Pseudomonas* sp. strain CA5. *Curr. Microbiol.* 58, 493–498. doi:10.1007/s00284-009-9358-2.
- Ike, M., Soda, S., Kuroda, M., 2017. Bioprocess approaches for the removal of selenium from industrial waste and wastewater by *Pseudomonas stutzeri* NT-1. In: *Bioremediation of Selenium Contaminated Wastewater*. Springer International Publishing, pp. 57–73. doi:10.1007/978-3-319-57831-6\_3.
- Jain, R., Seder-Colomina, M., Jordan, N., Dessi, P., Cosmidis, J., van Hullebusch, E.D., Weiss, S., Farges, F., Lens, P.N.L., 2015. Entrapped elemental selenium nanoparticles affect physicochemical properties of selenium fed activated sludge. *J. Hazard. Mater.* 295, 193–200. doi:10.1016/j.jhazmat.2015.03.043.
- Jin, W., Jiang, S., Pan, H., Tang, R., 2018. Amorphous phase mediated crystallization: fundamentals of biomineralization. *Crystals* 8, 48. doi:10.3390/cryst810048.
- Kim, H.-W., Hong, S.H., Choi, H., 2020. Effect of nitrate and perchlorate on selenate reduction in a sequencing batch reactor. *Processes* 8, 344. doi:10.3390/pr8030344.
- Knotek-Smith, H.M., Crawford, D.L., Möller, G., Henson, R.A., 2006. Microbial studies of a selenium-contaminated mine site and potential for on-site remediation. *J. Ind. Microbiol. Biotechnol.* 33, 897–913. doi:10.1007/s10295-006-0149-5.
- Lai, C.Y., Yang, X., Tang, Y., Rittmann, B.E., Zhao, H.P., 2014. Nitrate shaped the selenate-reducing microbial community in a hydrogen-based biofilm reactor. *Environ. Sci. Technol.* 48, 3395–3402. doi:10.1021/es4053939.
- Lemly, A.D., 2004. Aquatic selenium pollution is a global environmental safety issue. *Ecotoxicol. Environ. Saf.* 59, 44–56. doi:10.1016/S0147-6513(03)00095-2.
- Lenz, M., Enright, A.M., O'Flaherty, V., Van Aelst, A.C., Lens, P.N.L., 2009. Bioaugmentation of UASB reactors with immobilized *Sulfurospirillum barnesii* for simultaneous selenate and nitrate removal. *Appl. Microbiol. Biotechnol.* 83, 377–388. doi:10.1007/s00253-009-1915-x.
- Lenz, M., Hullebusch, E.D.V., Van, Hommes, G., Corvini, P.F.X., Lens, P.N.L., 2008a. Selenate removal in methanogenic and sulfate-reducing upflow anaerobic sludge bed reactors. *Water Res.* 42, 2184–2194.
- Lenz, M., Kolvenbach, B., Gygax, B., Moes, S., Corvini, P.F.X., 2011. Shedding light on selenium biomineralization: proteins associated with bionanominerals. *Appl. Environ. Microbiol.* 77, 4676–4680. doi:10.1128/AEM.01713-10.
- Lenz, M., Smit, M., Binder, P., van Aelst, A.C., Lens, P.N.L., 2008b. Biological alkylation and colloid formation of selenium in methanogenic UASB reactors. *J. Environ. Qual.* 37, 1691–1700. doi:10.2134/jeq2007.0630.
- Liamleam, W., Annachhatre, A.P., 2007. Electron donors for biological sulfate reduction. *Biotechnol. Adv.* doi:10.1016/j.biotechadv.2007.05.002.
- Lindeboom, R.E.F., Fermo, F.G., Weijma, J., Zagt, K., Van Lier, J.B., 2011. Autogenetic high pressure digestion: anaerobic digestion and biogas upgrading in a single step reactor system. *Water Sci. Technol.* 64, 647–653. doi:10.2166/wst.2011.664.
- Mal, J., Nancharaiyah, Y.V., van Hullebusch, E.D., Lens, P.N.L., 2017. Biological removal of selenate and ammonium by activated sludge in a sequencing batch reactor. *Bioresour. Technol.* 229, 11–19. doi:10.1016/j.biortech.2016.12.112.
- Michalke, K., Wickenheiser, E.B., Mehring, M., Hirner, A.V., Hensel, R., 2000. Production of volatile derivatives of metal(loid)s by microflora involved in anaerobic digestion of sewage sludge. *Appl. Environ. Microbiol.* 66, 2791–2796. doi:10.1128/AEM.66.7.2791-2796.2000.
- Mol, A., van der Weijden, R., Klok, J., Buisman, C., 2020. Properties of sulfur particles formed in biodesulfurization of. *Biogas. Minerals* 10, 433. doi:10.3390/min10050433.
- Nancharaiyah, Y.V., Lens, P.N.L., 2015. Ecology and biotechnology of selenium-respiring bacteria. *Microbiol. Mol. Biol. Rev.* 79, 61–80. doi:10.1128/MMBR.00037-14.
- Nasaringarao, P., Häggblom, M.M., 2007. *Pelobacter seleniigenes* sp. nov., a selenaterespiring bacterium. *Int. J. Syst. Evol. Microbiol.* 57, 1937–1942. doi:10.1099/ij.s.0.64980-0.
- Nelson, D.C., Casey, W.H., Sison, J.D., Mack, E.E., Ahmad, A., Pollack, J.S., 1996. Selenium uptake by sulfur-accumulating bacteria. *Geochim. Cosmochim. Acta* 60, 3531–3539. doi:10.1016/0016-7037(96)00221-9.
- Ontiveros-Valencia, A., Penton, C.R., Krajmalnik-Brown, R., Rittmann, B.E., 2016. Hydrogen-fed biofilm reactors reducing selenate and sulfate: community structure and capture of elemental selenium within the biofilm. *Biotechnol. Bioeng.* 113, 1736–1744. doi:10.1002/bit.25945.
- Ontiveros-Valencia, A., Zhou, C., Zhao, H.P., Krajmalnik-Brown, R., Tang, Y., Rittmann, B.E., 2018. Managing microbial communities in membrane biofilm reactors. *Appl. Microbiol. Biotechnol.* doi:10.1007/s00253-018-9293-x.
- Parikh, S.J., Chorover, J., 2008. ATR-FTIR study of lipopolysaccharides at mineral surfaces. *Colloids Surfaces B Biointerfaces* 62, 188–198. doi:10.1016/j.colsurfb.2007.10.002.
- Pearce, C.I., Coker, V.S., Charnock, J.M., Patrick, R.A.D., Mosselmans, J.F.W., Law, N., Beveridge, T.J., Lloyd, J.R., 2008. Microbial manufacture of chalcogenide-based nanoparticles via the reduction of selenite using *Veillonella atypica*: an in situ EXAFS study. *Nanotechnology* 19, 155603. doi:10.1088/0957-4484/19/15/155603.
- Pearce, C.I., Patrick, R.A.D., Law, N., Charnock, J.M., Coker, V.S., Fellowes, J.W., Oremland, R.S., Lloyd, J.R., 2009. Investigating different mechanisms for biogenic selenite transformations: geobacter sulfurreducens, *Shewanella oneidensis* and *Veillonella atypica*. *Environ. Technol.* 30, 1313–1326. doi:10.1080/0959330902984751.
- Rayman, M.P., 2012. Selenium and human health. *Lancet* 379, 1256–1268. doi:10.1016/S0140-6736(11)61452-9.
- Roest, K., Heilig, H.G.H.J., Smidt, H., De Vos, W.M., Stams, A.J.M., Akkermans, A.D.L., 2005. Community analysis of a full-scale anaerobic bioreactor treating paper mill wastewater. *Syst. Appl. Microbiol.* 28, 175–185. doi:10.1016/j.syapm.2004.10.006.
- Ruiken, C.J., Breuer, G., Klaversma, E., Santiago, T., van Loosdrecht, M.C.M., 2013. Sieving wastewater - cellulose recovery, economic and energy evaluation. *Water Res.* 47, 43–48. doi:10.1016/j.watres.2012.08.023.
- Schmitt, C., Sanchez, C., Desobry-Banon, S., Hardy, J., 1998. Structure and techno-functional properties of protein-polysaccharide complexes: a review. *Crit. Rev. Food Sci. Nutr.* doi:10.1080/10408699891274354.
- Staicu, L.C., Barton, L.L., 2017. Bacterial metabolism of selenium—for survival or profit. In: *Bioremediation of Selenium Contaminated Wastewater*. Springer International Publishing, Cham, pp. 1–31. doi:10.1007/978-3-319-57831-6\_1.
- Staicu, L.C., van Hullebusch, E.D., Lens, P.N.L., 2015. Production, recovery and reuse of bio-organic elemental selenium. *Environ. Chem. Lett.* doi:10.1007/s10311-015-0492-8.
- Stams, A.J.M., Grolle, K.C.F., Frijters, C.T.M.J., Van Lier, J.B., 1992. Enrichment of thermophilic propionate-oxidizing bacteria in syntrophy with *Methanobacterium thermoautotrophicum* or *Methanobacterium thermoformicum*. *Appl. Environ. Microbiol.* 58, 346–352.
- Switzer Blum, J., Burns Bindi, A., Buzzelli, J., Stolz, J.F., Oremland, R.S., 1998. *Bacillus arsenicoselenatis* sp. nov., and *Bacillus selenitireducens* sp. nov.: two haloalkaliphiles from Mono Lake, California that respire oxyanions of selenium and arsenic. *Arch. Microbiol.* 171, 19–30. doi:10.1007/s002030050673.
- Tan, L.C., 2018. Anaerobic Treatment of Mine Wastewater For the Removal of Selenate and Its co-contaminants, Anaerobic treatment of Mine Wastewater For the Removal of Selenate and Its Co-Contaminants. CRC Press doi:10.1201/9780429448676.
- Tan, L.C., Espinosa-Ortiz, E.J., Nancharaiyah, Y.V., van Hullebusch, E.D., Gerlach, R., Lens, P.N.L., 2018a. Selenate removal in biofilm systems: effect of nitrate and sulfate on selenium removal efficiency, biofilm structure and microbial community. *J. Chem. Technol. Biotechnol.* 93, 2380–2389. doi:10.1002/jctb.5586.
- Tan, L.C., Nancharaiyah, Y.V., Lu, S., van Hullebusch, E.D., Gerlach, R., Lens, P.N.L., 2018b. Biological treatment of selenium-laden wastewater containing nitrate and sulfate in an upflow anaerobic sludge bed reactor at pH 5.0. *Chemosphere* 211, 684–693. doi:10.1016/j.chemosphere.2018.07.079.
- Tan, L.C., Nancharaiyah, Y.V., van Hullebusch, E.D., Lens, P.N.L., 2016a. Selenium: environmental significance, pollution, and biological treatment technologies. *Biotechnol. Adv.* 34, 886–907. doi:10.1016/j.biotechadv.2016.05.005.
- Tan, Y., Yao, R., Wang, R., Wang, D., Wang, G., Zheng, S., 2016b. Reduction of selenite to Se(0) nanoparticles by filamentous bacterium *Streptomyces* sp. ES2-5 isolated from a selenium mining soil. *Microb. Cell Fact.* 15, 1–10. doi:10.1186/s12934-016-0554-z.
- Ter Heijne, A., De Rink, R., Liu, D., Klok, J.B.M., Buisman, C.J.N., 2018. Bacteria as an Electron Shuttle for Sulfide Oxidation. *Environ. Sci. Technol. Lett.* 5, 495–499. doi:10.1021/acs.estlett.8b00319.
- Ullah, H., Liu, G., Yousaf, B., Ali, M.U., Abbas, Q., Munir, M.A.M., Mian, M.M., 2018. Developmental selenium exposure and health risk in daily foodstuffs: a systematic review and meta-analysis. *Ecotoxicol. Environ. Saf.* 149, 291–306. doi:10.1016/j.ecoenv.2017.11.056.
- van Eerten-Jansen, M.C.A.A., Jansen, N.C., Plugge, C.M., de Wilde, V., Buisman, C.J.N., ter Heijne, A., 2015. Analysis of the mechanisms of bioelectrochemical methane production by mixed cultures. *J. Chem. Technol. Biotechnol.* 90, 963–970. doi:10.1002/jctb.4413.
- Van Ginkel, S.W., Yang, Z., Kim, B.o., Sholin, M., Rittmann, B.E., 2011. The removal of selenate to low ppb levels from flue gas desulfurization brine using the H<sub>2</sub>-based membrane biofilm reactor (MBFR). *Bioresour. Technol.* 102, 6360–6364. doi:10.1016/j.biortech.2011.03.010.
- Weijden, W.J.V.D., Hees, E., Bastein, T., Udo de Haes, H., van der Weijden, W.J., Hees, E., Bastein, T., de Haes, H.A.U., 2013. *The Geopolitics of Raw Materials For Agriculture and Food Production*. Platform Agriculture, Innovation & Society.

- Weijma, J., Stams, A.J.M., Hulshoff Pol, L.W., Lettinga, G., 2000. Thermophilic sulfate reduction and methanogenesis with methanol in a high rate anaerobic reactor. *Biotechnol. Bioeng.* 67, 354–363. doi:10.1002/(SICI)1097-0290(20000205)67:3<354::AID-BIT12>3.0.CO;2-X.
- Yoon, R.H., 1993. Microbubble flotation. *Miner. Eng.* 6, 619–630. doi:10.1016/0892-6875(93)90116-5.
- Zehr, J.P., Oremland, R.S., 1987. Reduction of selenate to selenide by sulfate-respiring bacteria: experiments with cell suspensions and estuarine sediments. *Appl. Environ. Microbiol.* 53, 1365–1369. doi:10.1016/0198-0254(87)96089-4.
- Zhang, Y., Zahir, Z.A., Frankenberger, W.T., 2004. Fate of colloidal-particulate elemental selenium in aquatic systems. *J. Environ. Qual.* 33, 559–564. doi:10.2134/jeq2004.5590.
- Hageman, S.P.W., van der Weijden, R.D., Stams, A.J.M., Buisman, C.J.N., Selenate reduction to produce recoverable selenium at 50°C by granular sludge from an anaerobic reactor; Chapter 4 in : Hageman, S.P.W., 2015. *Bio-induced solid selenium for recovery from water* (Doctoral dissertation), Wageningen University, ISBN 9789462575103 <https://library.wur.nl/WebQuery/wda/2101377>